Preliminary Evaluation of Anode-Layer-Type Hall Thruster Performance Using Pulsating Boost Chopper Circuit

IEPC-2019-752

Presented at the 36th International Electric Propulsion Conference
University of Vienna • Vienna, Austria
September 15-20, 2019

Kenshin Nagamine[1], Naoki Nozue[1], and Haruki Takegahara[2]
Tokyo Metropolitan University, Hino, Tokyo, 191-0065, Japan

Naoji Yamamoto[3]
Kyushu University, Kasuga, Hukuoka, 816-8580, Japan

and

Taichiro Tamida[4]
Mitsubishi Electric Corporation, Amagasaki, 661-8661, Jaoan

Abstract: In Hall thrusters, a discharge current oscillation has been an annoyance to extend a lifetime of both thrusters and power processing units (PPUs). In the discharge current oscillation, low-frequency oscillations are larger than the others and give rise to a plasma extinguishment. Moreover, an amplitude and dominant frequency of these oscillations vary as the change of operational conditions and thruster wear. These phenomena are the potential cause on the increase of a mass/volume at PPUs. To mitigate these drawbacks of the discharge current oscillation, a pulsating boost chopper circuit was developed. In past investigations, the controllability of oscillation frequency and improvements of thrust performance was confirmed. In this paper, applying the circuit for an anode-layer-type Hall thruster, we achieved the suppression of the oscillation amplitude and the wall erosion with almost the same thrust performance compared with constant voltage operation. Therefore, using a pulsating boost chopper circuit is promising for a future driving method of Hall thrusters.

Nomenclature

A_{f_c}	=	amplitude spectrum of chopping frequency at chopper operation
A_{f_n}	=	amplitude spectrum of natural frequency at DC operation
B_r	=	radial magnetic flux density on channel center line
D	=	duty ratio
f_c	=	chopping frequency
f_n	=	natural frequency at DC operation
I_d	=	discharge current
I_g	=	guard-ring current
$\dot{m}_a$	=	anode mass flow rate
P_d	=	discharge power

[1] Graduate Student, Department of Astronautics and Aeronautics, nagamine-kenshin@ed.tmu.ac.jp.
[2] Professor, Department of Astronautics and Aeronautics, h-takegahara@tmu.ac.jp.
[3] Professor, Department of Advanced Energy Engineering Science, yamamoto@aees.kyushu-u.ac.jp.
[4] Senior Researcher, Advanced Technology R&D Center, Tamida.Taichiro@aj.MitsubishiElectric.co.jp.

T	=	thrust
V_{base}	=	base voltage
V_d	=	discharge voltage
η_a	=	anode efficiency
τ	=	measurement time

I.Introduction

THE discharge current oscillation is one of the unique characteristics of Hall thrusters. Various instabilities of a discharge plasma affect an extensive frequency range oscillation[1] and these instabilities are propagated in different directions because particles with variety velocities exist in an acceleration channel. In the discharge current oscillation, low-frequency (1-100 kHz) range oscillations due to the ionization instability[1–3] are larger than that of the others and have been considered as the potential cause of discharge plasma extinguishment and shorter lifetime of Hall thrusters. The discharge current oscillation also has undesirable effects on power processing units (PPUs) for Hall thrusters because a PPU is typically developed to work under the condition of a constant voltage and constant current. To maintain the discharge plasma in Hall thrusters from BOL to EOL, PPUs must take a bigger margin for the wider frequency range and various amplitudes of the discharge current oscillation than expected. That is, the larger margin of PPUs leads to the larger mass, that reduces available payload masses of a satellite. Thus, at the aspect of mass, the larger discharge current oscillation is ultimately undesirable for spacecraft operation. Furthermore, the frequency and amplitude of the discharge current oscillation vary with a change of operational conditions and thruster wear. If a discharge current oscillates at unknown frequencies, it is also undesirable for other mission systems from the viewpoint of electromagnetic compatibility (EMC). Therefore, not only suppression of amplitudes but also a controllability of frequencies are required for the future Hall thruster driving systems. Some studies that specifically aim to suppress the low-frequency oscillations have conducted to investigate its mechanism[4,5]. However, none of them was able to achieve the suppression of the oscillations completely.

In recent years, an all-electric satellite and maned deep space mission gather increasing attention in the world. Therefore, it will be more important to reduce the mass of the PPU. However, employing a conventional DC power supply, the mass/volume of the PPU increases with the development of high-power Hall thrusters. As one of the solutions for the above drawbacks of the discharge current oscillation, Tamida et al.[6] and Yamamoto et al.[7,8] developed “harmonized PPU,” that installs a pulsating boost chopper circuit which can provide a fluctuated voltage as a discharge voltage of Hall thrusters. They applied the chopper circuit for a low-power operation of 1-kW class magnetic-layer-type Hall thruster developed at Kyushu University. The fluctuated voltage produced by the pulsating boost chopper circuit enables the discharge voltage to synchronize with discharge current oscillations and can control the frequencies in various magnetic field strength.[6–8] Using the chopper circuit, the controllability of the low-frequency oscillation has been confirmed and has made improvements on a thrust efficiency and thrust-to-power ratio. Moreover, the pulsating boost chopper circuit doesn’t require a high capacitance smoothing capacitor and isolation transformer, which lead to the mass reduction of PPUs. As described above, it is beneficial for the operation of Hall thrusters to apply the pulsating boost chopper circuit for that’s PPUs.

However, the data for the operation with the pulsating boost chopper circuit are still not enough. Furthermore, a demonstration with an anode-layer-type Hall thruster has never conducted. Thus, applying the pulsating boost chopper circuit for a 1-kW class anode-layer-type Hall thruster, the objectives in this study are to evaluate thrust performance, to confirm the controllability for the frequency of discharge current oscillation, and to investigate the operational characteristics such as current-voltage waveform and frequency characteristics.

II.Experimental Apparatus and Procedure

A. Anode-Layer-Type Hall Thruster

Figure 1 shows a schematic illustration of the 1-kW class anode-layer-type Hall thruster (TMU-066) developed at Tokyo Metropolitan University and Fig. 2 shows the maximum radial magnetic flux density on the channel centerline as a function of the axis position. TMU-066 employs a hollow anode made of copper. The inner diameter and outer radius of the acceleration channel are 19 mm and 33 mm respectively. The magnetic circuit consists of an inner/outer coil and the back/front plate made of soft iron. The insulators are made of alumina, and the guard-rings are made of stainless steel (SUS316L). A propellant is temporarily stored and is fed to the acceleration channel through the uniform 24 holes on the azimuthal direction. As shown in Fig. 2, the radial magnetic flux density reaches the maximum value at the channel exit plane. The inner coil current, I_{ci}, was fixed at one-quarter of the outer coil current, I_{co}, through entire experiments.

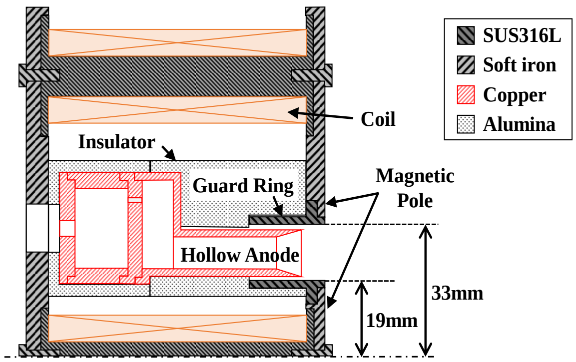

Figure 1. Cross section of the anode-layer-type Hall thruster developed at Tokyo Metropolitan University (TMU-066).

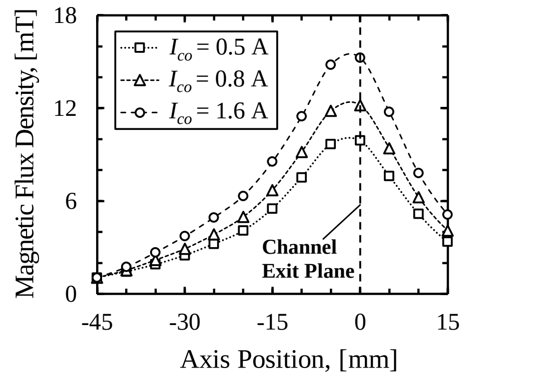

Figure 2. Maximum radial magnetic flux density on channel center line as a function of axis direction.

B. Pulsating Boost Chopper Circuit

Figure 3 shows a schematic representation of circuit A (pulsating boost chopper circuit) and circuit B. Circuit parameters consist of a base voltage, V_{base}, a discharge voltage, V_d, input capacitance, C_{in}, inductance of reactor, L, output capacitance, C_{out}, and the metal-oxide-semiconductor field-effect transistor (MOSFET). A function generator produces a chopping frequency, f_c, and duty ratio, D, to switch the MOSFET. The unique characteristic of this circuit is to use low output capacitance on purpose to provide a fluctuated voltage. In this paper, we conducted entire experiments as changing a chopping frequency and output capacitance. The other parameters were fixed as follows; C_{in} = 2.2 μF, L = 0.5 mH, D = 0.33. As for circuit B, a base voltage, V_{base}, equals a discharge voltage, V_d, because there is no reactor, L, output capacitance, C_{out}, and signals from a function generator (chopping frequency, f_c, and duty ratio, D).

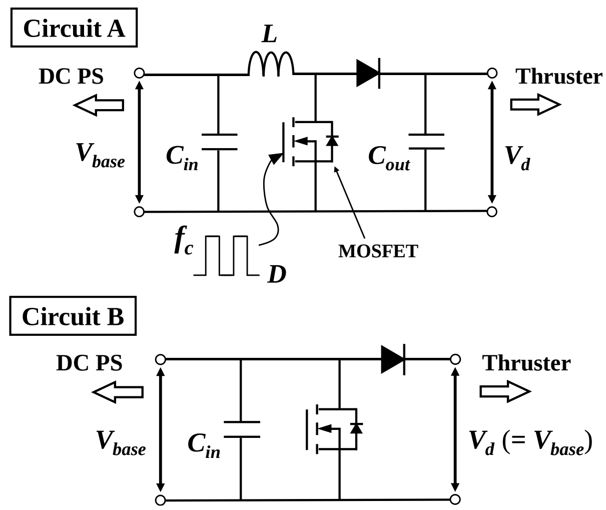

Figure 3. Circuit A (pulsating boost chopper circuit) and Circuit B.

C. Experimental Setup

Figure 4 shows an electrical diagram of the anode-layer-type Hall thruster. All experiments in this paper conducted in the vacuum chamber whose length is 3.2 m and the diameter is 1.6 m. The minimum background pressure is approximately 0.5×10^{-4} Pa and kept under than 8.0×10^{-3} Pa through all experiment. We used the xenon (99.999% pure) as a propellant. A discharge current, I_d, guard-ring current, I_g, and discharge voltage, V_d, were measured by the current probe and oscilloscope (Tektronix, Inc., the current probe : TCP-312 and TCPA-300, the oscilloscope : TDS2014B). These above values (I_d, I_g, and V_d) were calculated as an average of the measured value and sampling time was 5 ms. A cathode's potential was floated from GND to neutralize the ion beam with only electrons provided by the hollow cathode.

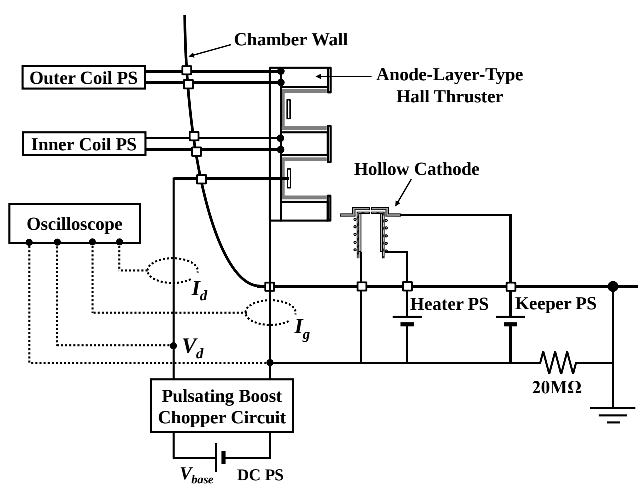

Figure 4. Electrical diagram of anode-layer-type Hall thruster.

III. Experimental Results and Discussions

In this paper, we refer to the operation of Hall thrusters using a DC power supply as "DC operation" and using a pulsating boost chopper circuit as "chopper operation."

A. Frequency Characteristics of Chopper Operation

In order to investigate the characteristics of chopper operation, we applied a pulsating boost chopper circuit for three different operating points as shown in Table 1, and Fig. 5 shows discharge voltage and discharge current characteristics for each operating point. To reduce measurement errors due to power losses in the circuit, these data for DC operation shown in Table 1 and Fig. 5 were obtained through the circuit B in Fig. 3. The discharge currents of these operating points naturally fluctuate, and the oscillation frequencies are different respectively due to each operational condition such as an input power, mass flow rate, and magnetic flux density.

Table 1. Operational condition of three operating points for DC operation with circuit B in Fig. 3.

Operating Point No.	1	2	3
Discharge Voltage, V_d	150 V	300 V	400 V
Anode Mass Flow Rate, $\dot{m}_a$	1.5 mg/s	2.0 mg/s	3.0 mg/s
Magnetic Flux Density, B_r	9.9 mT	15.3 mT	12.2 mT
Natural Frequency, f_n	8 kHz	18 kHz	32 kHz

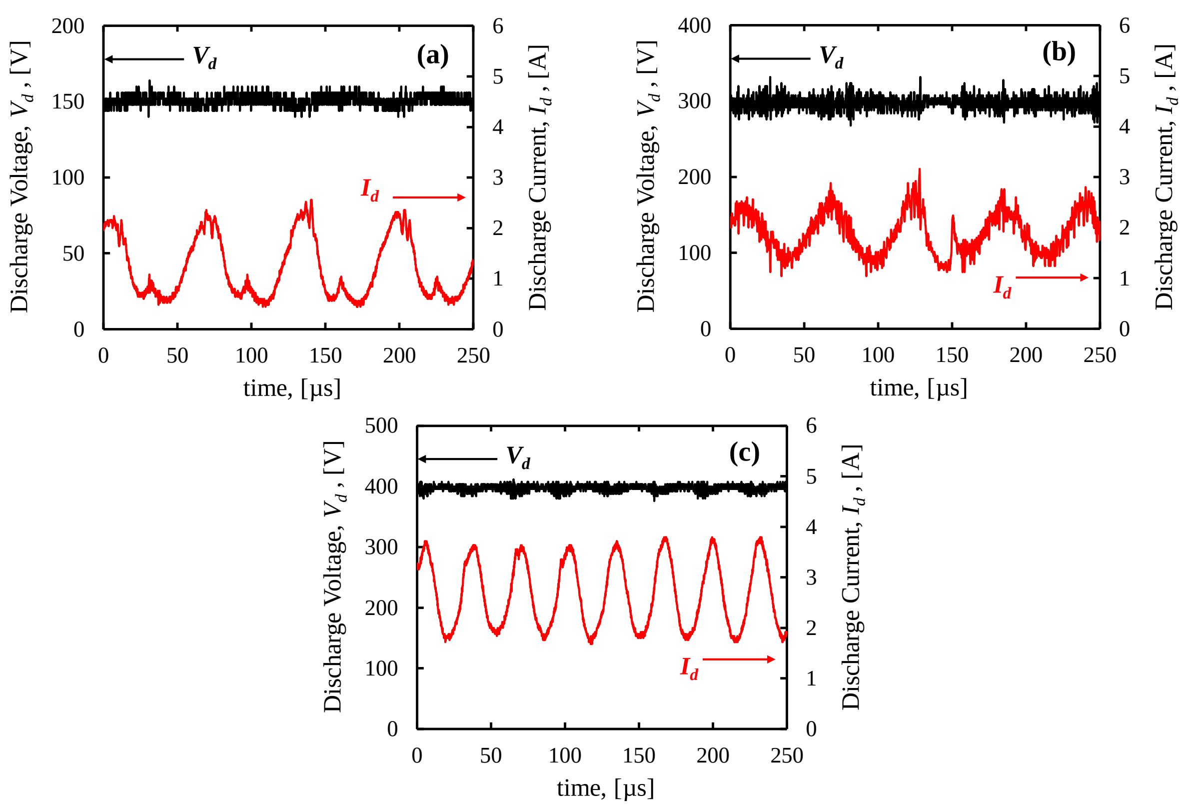

Figure 5. Discharge voltage and discharge current characteristics at DC operation; (a) Operating point 1, (b) Operating point 2, (c) Operating point 3.

At chopper operation, a discharge voltage, V_d, was adjusted by setting the base voltage, V_{base}, following the equation,

$$V_d = \frac{1}{1+D} V_{base} \tag{1}$$

where D is a duty ratio of a function generator. In the previous study for chopper operation[6-8], the base voltage was fixed through the entire experiments. However, when the base voltage, V_{base}, is adjusted to obtain an aimed discharge voltage, V_d, based on Eq. (1), the practical value of the discharge voltage, V_d, does not completely follow Eq. (1). The cause of this phenomenon results from the discontinuous conduction mode of the pulsating boost chopper circuit due to the impedance fluctuation of Hall thrusters because Eq. (1) assumes only the continuous conduction mode. Despite a minor change of the discharge voltage, the characteristics of a discharge current oscillation varies sensitively. In this paper, therefore, the discharge voltage, V_d, was fixed through the entire experiments to investigate the consistent characteristics of chopper operation.

Figures 6-8 show the discharge voltage and discharge current characteristics by chopper operation at each operating point with various chopping frequencies. The output capacitance is 0.47 μF for operating point 1 and 0.22 μF for operating points 2 and 3. The other circuit parameters, the input capacitance, C_{in}, inductance, L, and duty ratio, D, were fixed in the all experiments as follows; $C_{in} = 2.2$ μF, $L = 0.5$ mH, $D = 0.33$, respectively.

Normal operation was confirmed for chopper operation at various chopping frequencies. However, in the case of the operations at less than minimum chopping frequency at each operating point as shown in Figs. 6-8, a MOSFET or diode was broken by over-current; The detailed cause of these failures is uncertain. As shown in Figs. 6-8, the amplitude of discharge voltage decreases as the increase of the chopping frequency because energy accumulated in the reactor decreases due to the short switching cycle. As the discharge voltage decreases, the amplitude of the discharge current also decreases. Although it is confirmed that a coincidence on the oscillation frequency between the discharge voltage and discharge current at the chopping frequencies of 28, 40 and 48 kHz, it isn't established at 72 kHz as shown in Fig. 8. In order to clarify this phenomenon at chopper operation, we conducted a fast Fourier transform (FFT) for the discharge current oscillations and investigated frequency characteristics.

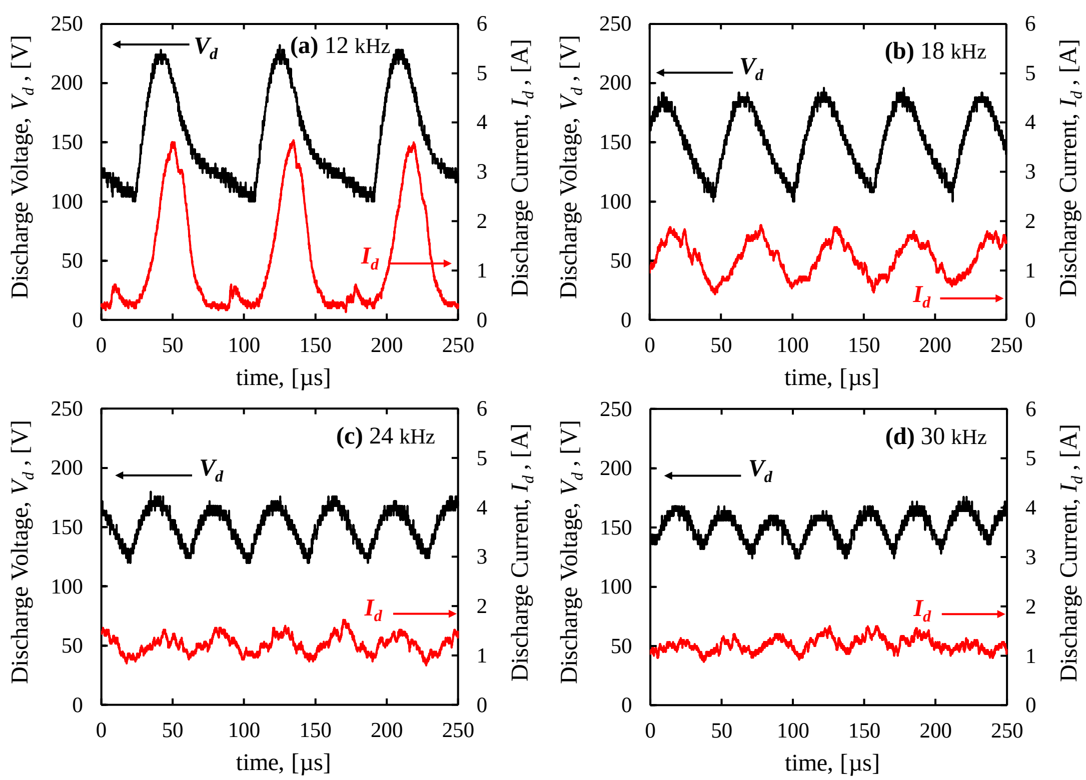

Figure 6. Discharge voltage and discharge current characteristics at operating point 1 in Fig. 5(a) by chopper operation with various chopping frequencies using circuit A in Fig. 3; (a) 12 kHz, (b) 18 kHz, (c) 24 kHz, (d) 30 kHz.

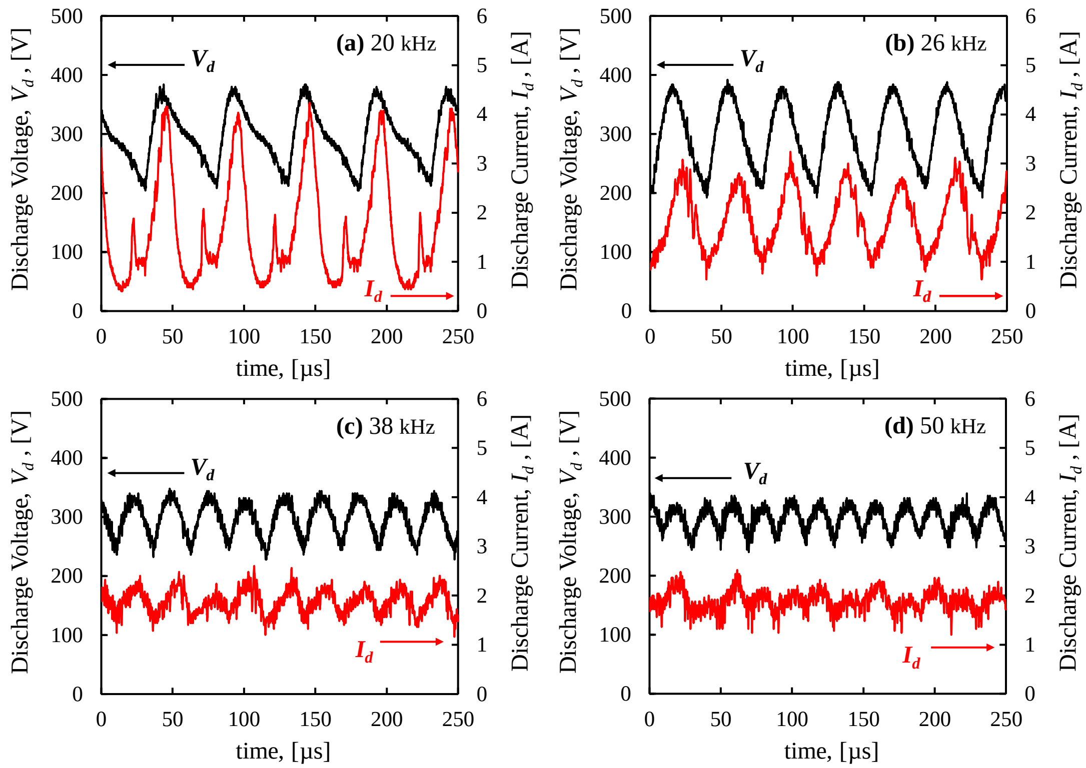

Figure 7. Discharge voltage and discharge current characteristics at operating point 2 in Fig. 5(b) by chopper operation with various chopping frequencies using circuit A in Fig. 3; (a) 20 kHz, (b) 26 kHz, (c) 38 kHz, (d) 50 kHz.

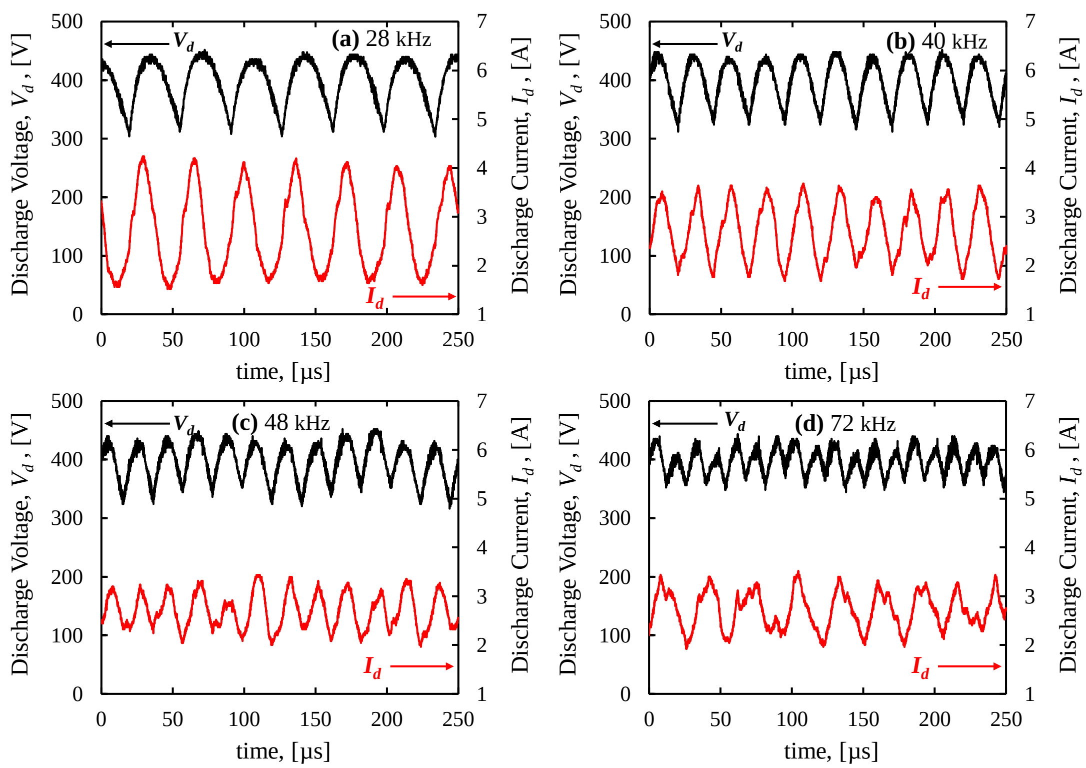

Figure 8. Discharge voltage and discharge current characteristics at operating point 3 in Fig. 5(c) by chopper operation with various chopping frequencies using circuit A in Fig. 3; (a) 28 kHz, (b) 40 kHz, (c) 48 kHz, (d) 72 kHz.

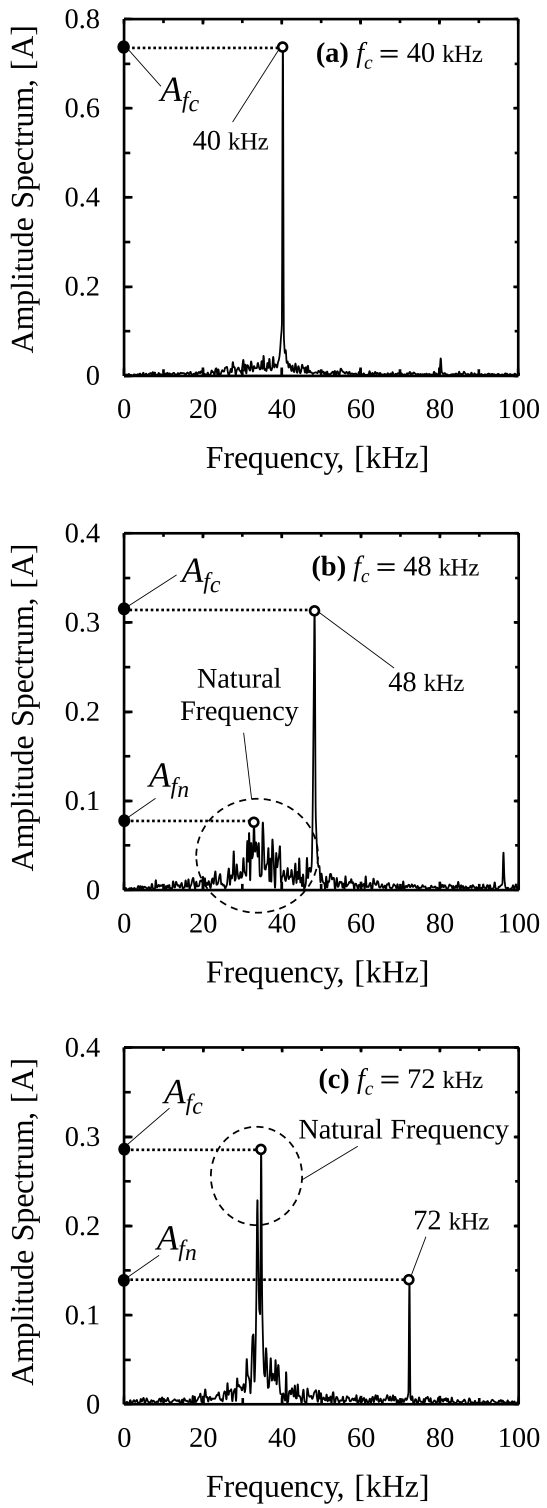

Figure 9. Amplitude spectrum of discharge current at chopper operation for operating point 3 with three chopping frequencies; (a) 40 kHz, (b) 48 kHz, (c) 72 kHz.

Figure 9 shows the amplitude spectrums of discharge current from FFT at operating point 3 for three chopping frequencies. At first, as shown in Fig. 9 (a), a dominant frequency of the discharge current oscillation corresponds to the chopping frequency, f_c. Next for Fig 9 (b), although the dominant frequency still corresponds to the chopping frequency, the frequencies around the natural frequency, f_n, of 32 kHz at DC operation appeared. At Fig. 9 (c), the natural frequencies overcome the chopping frequency and finally become the dominant frequency. In other words, a synchronization of the oscillation frequency between the discharge voltage and discharge current is lost as the increase of the chopping frequency. One of the benefits of applying a pulsating boost chopper circuit for Hall thrusters is to be able to control the dominant current oscillation frequency to chopping frequency with initiative. Thus, the synchronization among discharge voltage and discharge current is indispensable because it is effective for EMC and the suppression of the current oscillation discussed later in subsection C. In this paper, the condition of the synchronization between the discharge voltage and discharge current at chopper operation is defined as the following conditional equation,

$$A_{f_o} < \frac{A_{f_c}}{2} \tag{2}$$

where A_{f_o} is the amplitude spectrum at natural frequency and A_{f_c} is the amplitude spectrum at the chopping frequency as shown in Fig 9. According to Eq.(2), the synchronized chopping frequency ranges at chopper operation for each operating point are shown in Table 2. A synchronization range of a chopping frequency extends as the increase of an output capacitance due to a peak-peak discharge voltage becomes large even though it is at the same thruster condition as shown in Fig. 10. Moreover, compared with operating points 2 and 3 at the output capacitance of 0.22 μF, the synchronization range also extends as the increase of the discharge voltage because the peak-peak discharge voltage becomes large.

As a summary of frequency characteristics, a controllability for the frequency of discharge current oscillation was achieved at the certain chopping frequency range as shown in Table. 2. However, at a relatively high-frequency range, the discharge current is unsynchronized with the discharge voltage, which indicates that there is an optimal chopping frequency range for chopper operation. To find out the correlation among optimal frequency range and the other circuit parameters is one of the future works.

Table 2. Synchronized frequency ranges at chopper operation of each operating points for various output capacitances.

Operating Point	Discharge Voltage, V_d	Output Capacitance, C_{out}	Synchronized Range, f_c
1	150 V	0.47 μF	12 – 24 kHz
2	300 V	0.47 μF	18 – 26 kHz
		0.22 μF	20 – 38 kHz
3	400 V	0.22 μF	28 – 52 kHz

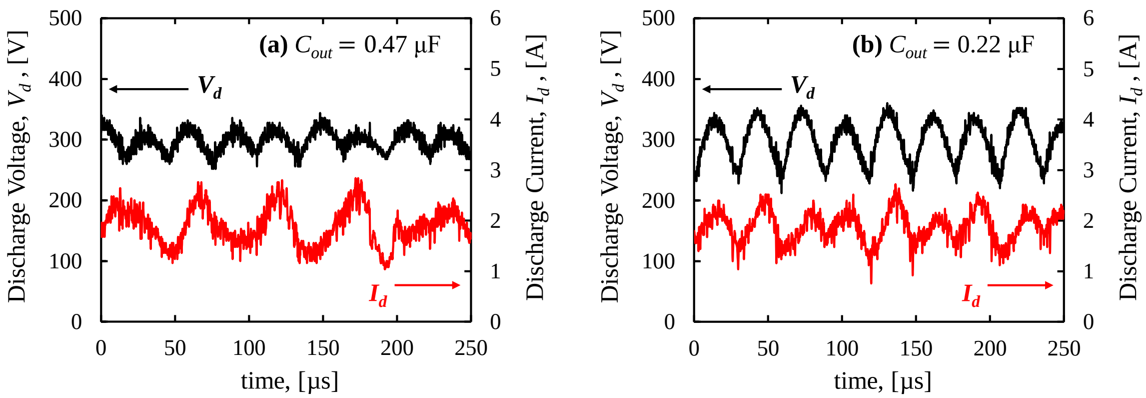

Figure 10. Discharge voltage and discharge current characteristics for chopper operation at operating point 2 regarding two output capacitances, C_{out}; (a) C_{out} = 0.47 μF, (b) C_{out} = 0.22 μF.

B. Thrust Performance of Chopper Operation

Figure 11 represents the thrust performances as a function of chopping frequency for each operating point; the data of DC operation are plotted at "DC" on the axis of a chopping frequency as black-closed symbols. An anode efficiency, η_a, was calculated as follows,

$$\eta_a = \frac{1}{2}\frac{T^2}{\dot{m}_a P_d} \tag{3}$$

where T is a thrust, $\dot{m}_a$ is an anode mass flow rate, and P_d is power consumption calculated as a product of a discharge voltage, V_d, and discharge current, I_d. A thrust to power ratio, T/P_d, was calculated as the ratio of a thrust, T, and power consumption, P_d.

At operating point 1 as shown in Fig. 11 (a), the thrust, the power consumption, and the anode efficiency decrease with the increase of a chopping frequency, and finally they are almost constant at a high chopping frequency range. At a low-frequency range, a larger peak value both the discharge voltage and discharge current due to shorter switching cycle results in larger power consumption, and the number of ions accelerated at a high voltage region increases. Given the above background, the thrust at a low chopping frequency is also larger than that at a high chopping frequency range and finally, the anode efficiency also increases at a low chopping frequency range. However, the T/P_d at chopper operation is lower than that at DC operation.

At operating point 2 as shown in Fig. 11 (b), the thrust, the power consumption, the T/P_d, and the anode efficiency are not remarkably changed over the chopping frequency of 26 kHz. On the other hand, at the chopping frequency below 26 kHz, the power consumption decreases with the decrease of chopping frequency and becomes lower than that at DC operation. This result causes the significant improvement of the T/P_d at a low chopping frequency range. However, there is no reliable evidence on the significant decrease in the power consumption. Hence, to investigate this phenomenon will be future work.

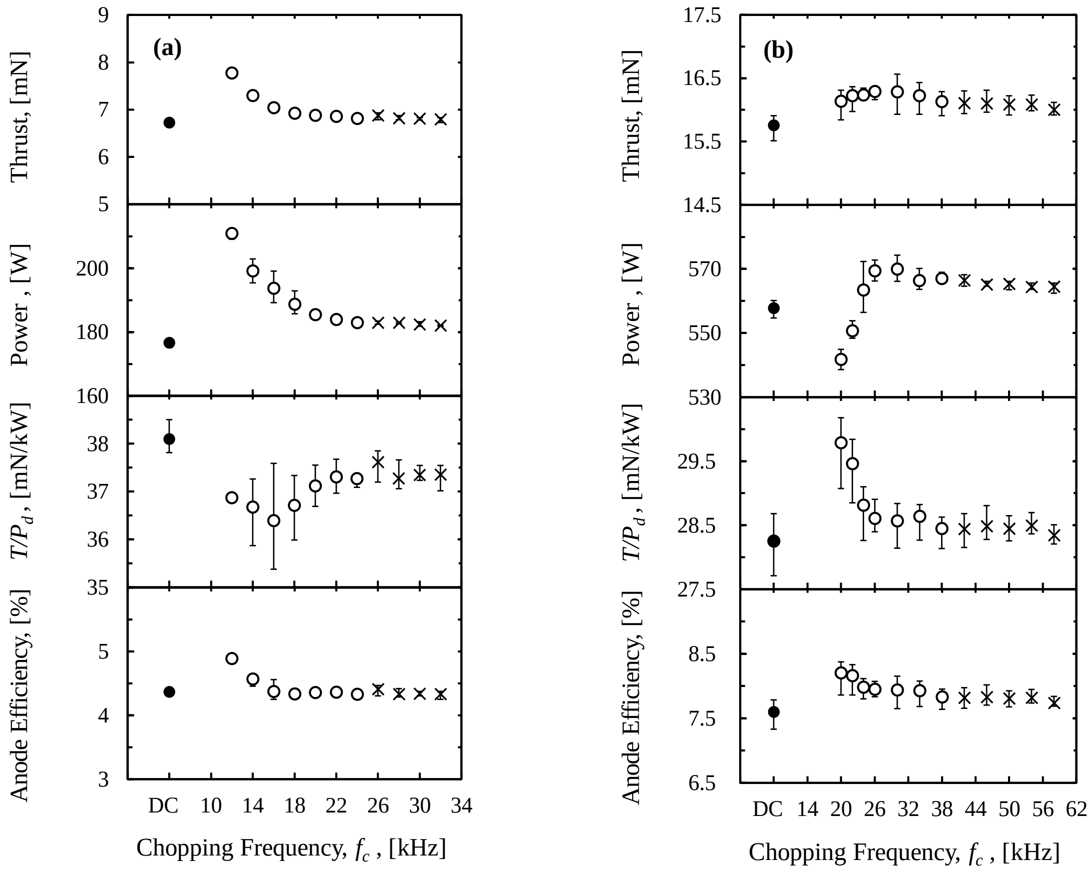

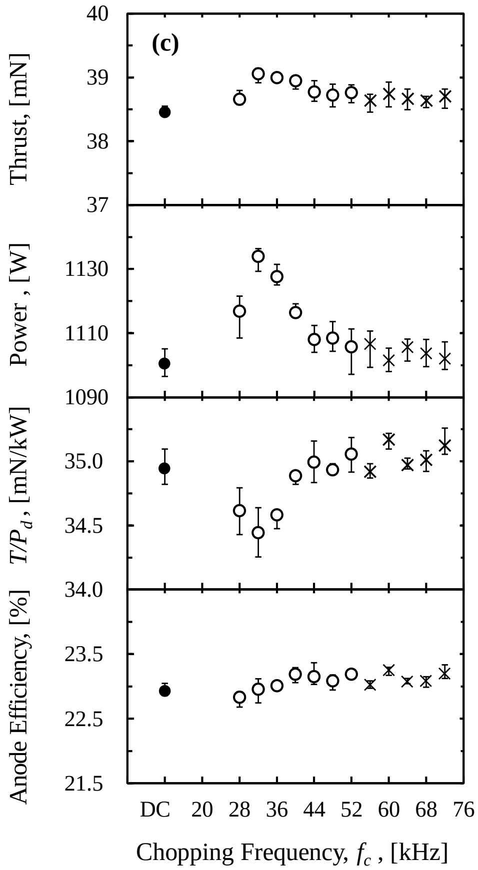

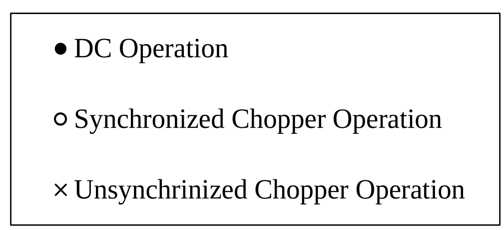

Figure 11. Thrust performance as a function of chopping frequency for each operating point; (a) Operating point 1, (b) Operating point 2, (c) Operating point 3.

At operating point 3 as shown in Fig. 11 (c), the thrust and the power consumption decrease as the increase of the chopping frequency except the data at 28 kHz. Whereas, contrary to operating point 1, the anode efficiencies at the chopping frequency of 28-38 kHz are a little bit lower than that at the other frequencies due to the bigger power consumption. Although the T/P_d over 40 kHz is comparable with DC operation, those below 36 kHz are lower than DC operation. Focussing on the thrust and power consumption at the chopping frequency of 28 kHz, those are lower than that of 32 kHz. A possible cause of this result is considered that most of the ions are not accelerated when a high voltage is applied because the phase of the discharge current leads from that of the discharge voltage.

As a summary, the thrust performance of chopper operation was almost the same as DC operation. As for operating point 2 at the chopping frequency of 20 and 22 kHz, the improvements of the thrust to power ratio, T/P_d, and the anode efficiency, η_a, were achieved compared with DC operation.

C. Oscillation Amplitude and Guard-Ring Current Ratio

An amplitude of a discharge current oscillation, Δ, and a guard-ring current ratio are introduced as indicators of chopper operation, and above two indicators are described as follows,

$$\Delta = \frac{\text{R.M.S.}}{\overline{I}_d} = \frac{1}{\overline{I}_d}\sqrt{\frac{\int_0^\tau (I_d - \overline{I}_d)^2\,dt}{\tau}}\ ,\ \left(\overline{I}_d = \frac{\int_0^\tau I_d\,dt}{\tau}\right) \tag{4}$$

$$\text{Guard-Ring Current Ratio} = \frac{\overline{I}_g}{\overline{I}_d}\ ,\ \left(\overline{I}_g = \frac{\int_0^\tau I_g\,dt}{\tau}\right) \tag{5}$$

where I_d is a discharge current, I_g is a guard-ring current and τ is a measurement time. In this paper, all averaged values were calculated with the measurement time of 5 ms.

The smaller amplitude of discharge current oscillation is the better for a stable operation of both thrusters and PPUs, in terms of a discharge extinguishment, an EMC, and the mass/volume of PPUs. The smaller guard-ring current ratio is also the better as the aspect of a thruster lifetime because, in the case of anode-layer-type Hall thrusters, the large guard-ring current ratio directly indicates the large plume divergence, wall erosion, and ion losses to the acceleration channel wall. Moreover, the large plume expansion is undesirable for spacecraft operations. For instance, a spacecraft surface is sputtered by impingement of high energy ions, and sputtered materials deposit on other surfaces, that can lead to change material characteristics. Furthermore, back flowed charge-exchange ions possibly give rise to an anomalous discharge on the surface of solar array panels. From the above reasons, the smaller both the amplitude of discharge current oscillation and the guard-ring current ratio, the better for both Hall thrusters and spacecrafts.

Figures 12-14 show the oscillation amplitude and guard-ring current ratio for each operating point. There is a decreasing tendency in the oscillation amplitude as the increase of the chopping frequency for each operating point. As for operating point 3, the amplitude for the chopping frequency of 28 kHz is smaller than that of 32 kHz. This result is considered that the ions are not accelerated at a high voltage region due to the phase difference between discharge current and discharge voltage as shown in Fig. 8(a). At the unsynchronized frequency range of operating point 3 (represented crossed-symbols), the oscillation amplitude increases as the increase of a chopping frequency. That is because, as shown in Fig. 9, the amplitude of the natural frequency oscillation gradually grows and becomes dominant. For all operating points, it was confirmed that the minimum oscillation amplitudes at chopper operation are smaller than those at DC operation. At operating points 1 and 3, there is also the decreasing tendency in the guard-ring current ratio against the increase of the chopping frequency except the 12 kHz at operating point 1 as shown in Figs. 12 and 14. Although, at operating point 2 over the chopping frequency of 28 kHz, there is a decreasing tendency as with operating points 1 and 3, the guard-ring current ratio under 20 kHz is smaller than that of DC operation. The details of the possible cause for this phenomenon is future work.

In summary of the effects on the above two indicators, the suppressions compared with DC operation were achieved in three operating points. Specifically, in operating point 3, the guard-ring current ratio was suppressed to half compared with DC operation. This result supposes that it is possible to extend a thruster lifetime using the chopper circuit.

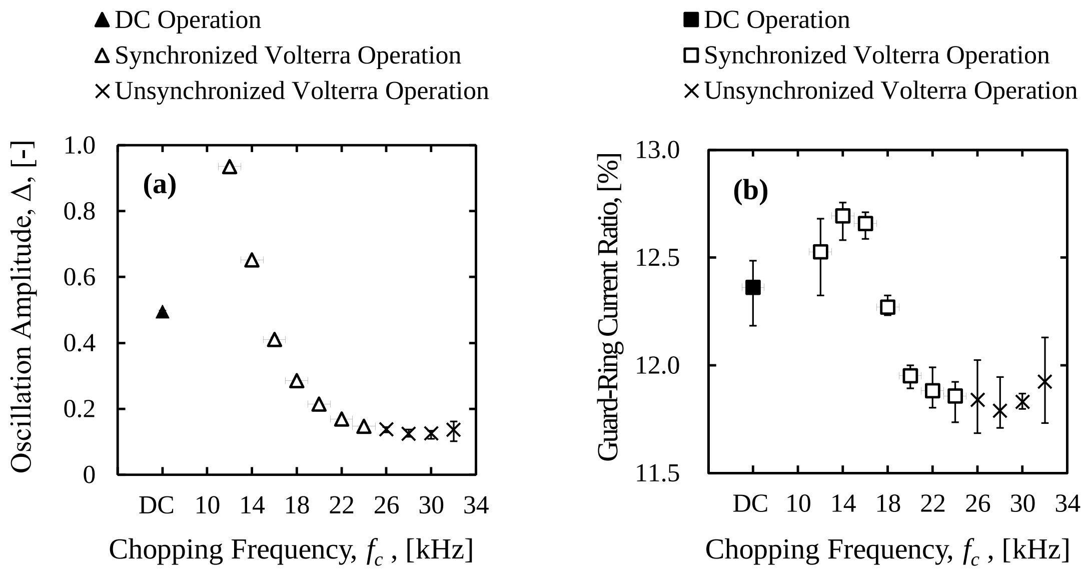

Figure 12. (a) Oscillation amplitude and (b) guard-ring current ratio as a function of chopping frequency for operating point 1 in Fig. 5(a).

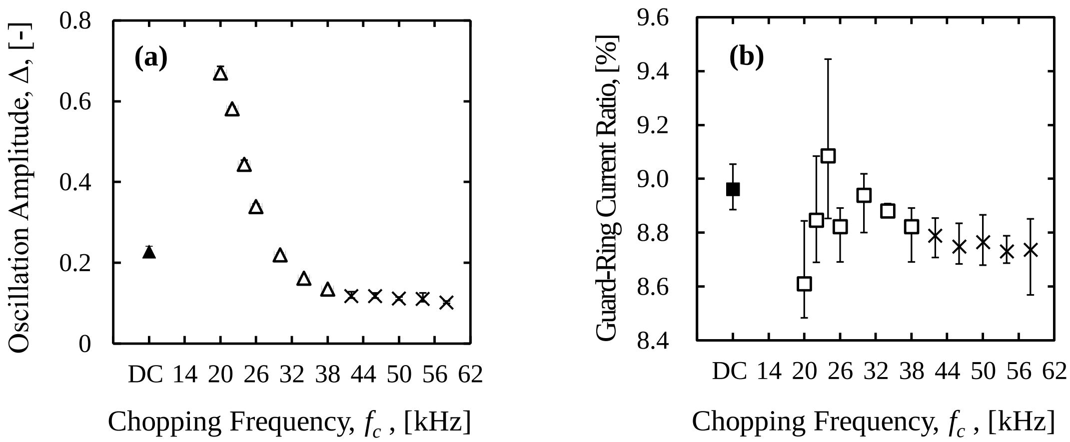

Figure 13. (a) Oscillation amplitude and (b) guard-ring current ratio as a function of chopping frequency for operating point 2 in Fig. 5(b).

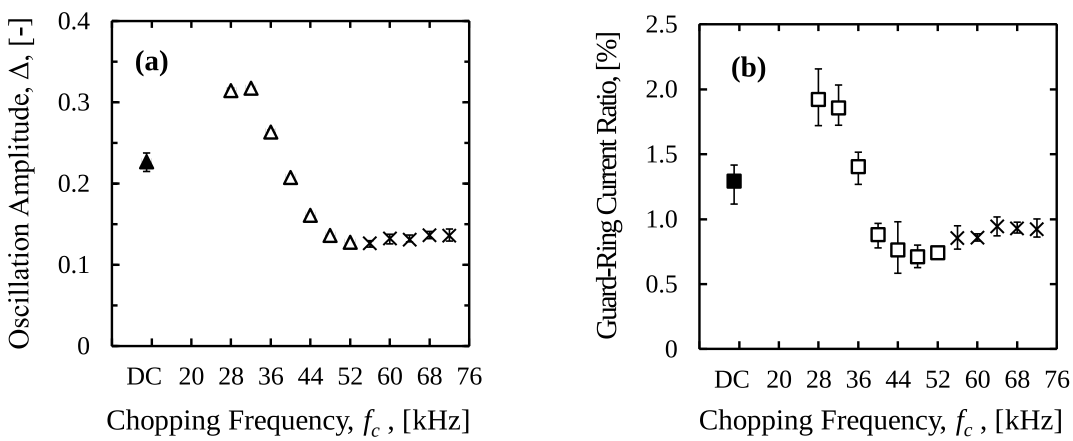

Figure 14. (a) Oscillation amplitude and (b) guard-ring current ratio as a function of chopping frequency for operating point 3 in Fig. 5(c).

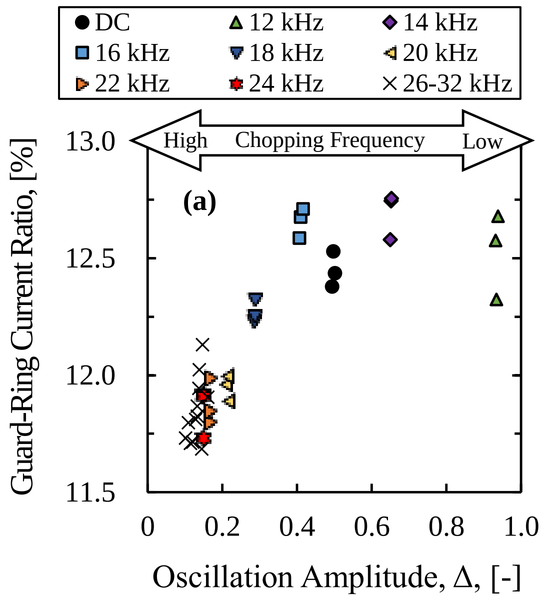

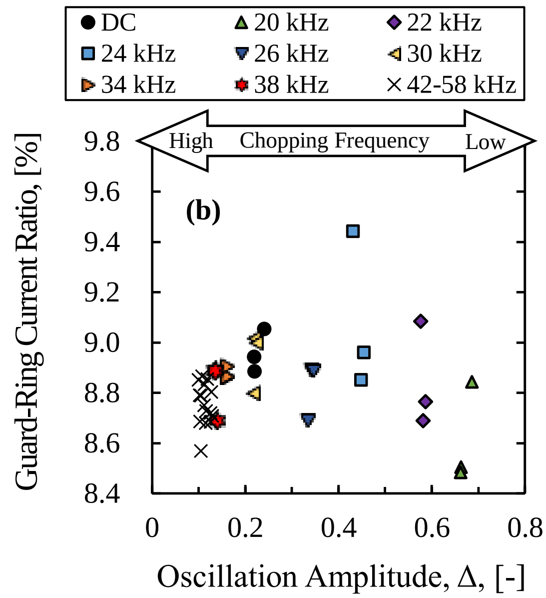

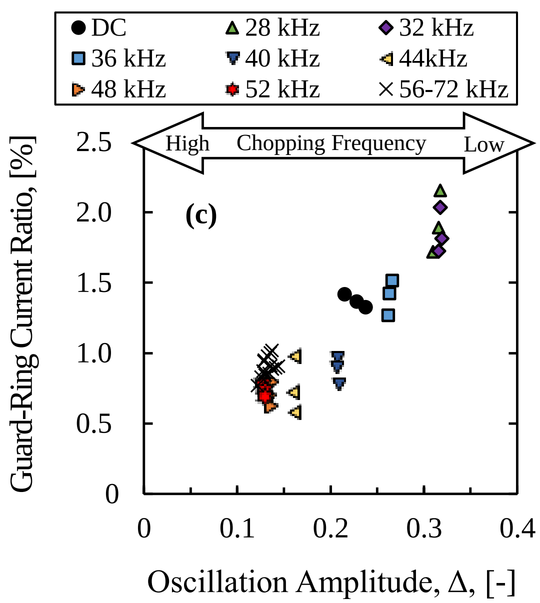

Figure 15. Guard-ring current ratio vs. oscillation amplitude with various chopping frequencies; (a) Operating point 1, (b) Operating point 2, (c) Operating point 3.

As described above, the decreasing tendency on the oscillation amplitude and guard-ring current ratio with the increase of a chopping frequency was confirmed, that suggests the reliable correlation between the two indicators. Figure 15 shows the correlation between the guard-ring current ratio and oscillation amplitude for each operating point. As for operating points 1 and 3, as shown in Fig.15(a) and Fig.15(c), there is an apparent positive correlation between the two indicators. That is, the larger discharge current oscillation is a potential cause of larger guard-ring current ratio. A possible physical background of this positive correlation can be described as follows; Figure 16 shows the characteristics of the guard-ring current, I_g, and discharge current, I_d, and the coincidence of the frequency between the two waves was confirmed. Moreover, compared with Fig. 16(a) and (b), the amplitude of the guard-ring current decreases as the decrease of the discharge current amplitude. Those results indicate that the guard-ring current also fluctuates with discharge current oscillation in relation to both the amplitude and frequency. Assuming a "predator-prey model[6]," the larger peak value of the discharge current leads to the larger number of ions accelerated at the peak current region. That is, we consider that ions accelerated toward the radial direction also increase with the increase of ions accelerated at the same time. Moreover, even though the discharge current is unsynchronized with the discharge voltage as shown in Fig. 17 that shows the discharge voltage, V_d, discharge current, I_d, and guard-ring current, I_g, waveforms at the unsynchronized chopping frequency of 72 kHz, the guard-ring current is synchronized with only the discharge current. In other words, the fluctuation of the discharge voltage does not contribute to the fluctuation of the guard-ring current. Thus, applying a pulsating boost chopper circuit to Hall thrusters does not directly influence the shorter lifetime of Hall thrusters because only the discharge current oscillation affects the guard-ring current ratio under the condition of constant magnetic field strength.

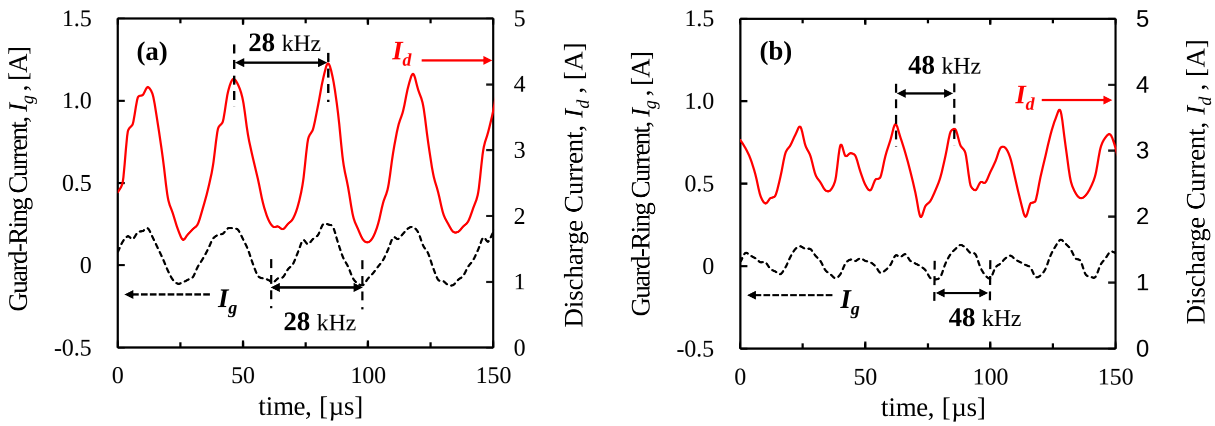

Figure 16. Guard-ring current and discharge current characteristics at operating point 3 in Fig. 5(c) for synchronized chopper operation; chopping frequencies of (a) 28 kHz, (b) 48 kHz.

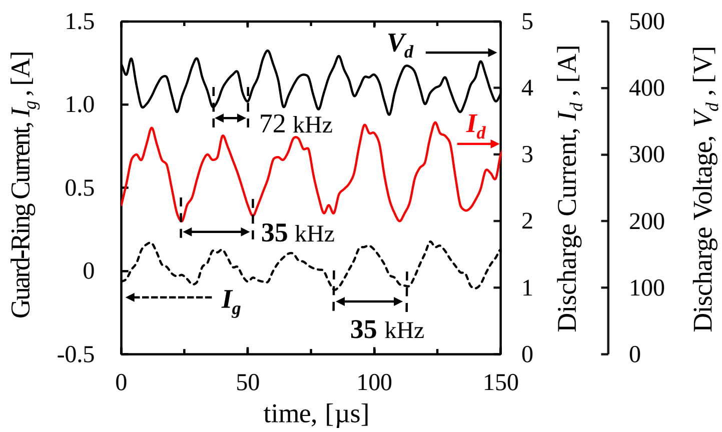

Figure 17. Guard-ring current, discharge current and discharge voltage characteristics at operating point 3 in Fig. 5(c) for unsynchronized chopper operation; chopping frequencies of 72 kHz.

IV.Conclusion

Normal operation was demonstrated using pulsating boost chopper circuit for a 1-kW class anode-layer-type Hall thruster. In addition to the potential benefits of the chopper circuit which can increase the available payload masses because of the absence of high capacitance capacitor, we achieved follows;

1) A controllability for the frequency of the discharge current oscillation was achieved.
2) It was possible to suppress the amplitude of the discharge current oscillation and guard-ring current ratio compared with DC operation. Specifically, at operating point 3, the guard-ring current ratio was suppressed to half compared with DC operation.
3) Improvements of thrust performance such as the thrust to power ratio and the anode efficiency were achieved at operating point 2, and the thrust performances at other operating points were almost the same as DC operation.

Furthermore, we found out that the discharge voltage fluctuation does not contribute to the guard-ring current oscillation, and only discharge current oscillation affects it. That is, applying a pulsating boost chopper circuit for Hall thrusters does not directly influence the guard-ring current which is the indicator of a plume divergence, wall erosion, and ion losses to an acceleration channel wall. Therefore, this new driving method using a pulsating boost chopper circuit is promising for future Hall thruster systems.

Acknowledgments

The authors would like to thank Dr. K. Kuriki (Professor Emeritus, Institute of Space and Astronautical Science) for helpful discussions and Dr. H. Watanabe (Assistant Professor, Tokyo Metropolitan University) for his assistances in experiments.

References

[1] Choueiri, E. Y., "Plasma oscillations in Hall thrusters," *Physics of Plasmas*, **8**, 1411–1426, 2001.

[2] Boeuf, J. P., "Tutorial: Physics and modeling of Hall thrusters," *Journal of Applied Physics*, **121**, 011101, 2017.

[3] Yamamoto, N., Komurasaki, K. & Arakawa, Y., "Discharge Current Oscillation in Hall Thrusters," *Journal of Propulsion and Power*, **21**, 870–876, 2005.

[4] Yamamoto, N., Yokota, S., Watanabe, K., Sasoh, A., Komurasaki, K. & Arakawa, Y., "Suppression of Discharge Current Oscillations in a Hall Thruster," *Transactions of the Japan Society for Aeronautical and Space Sciences*, **48**, 169–174, 2005.

[5] Furukawa, T., Miyasaka, T. & Fujiwara, T., "Methods of Controlling Low-Frequency Oscillation in a Hall Thruster," *27th International Electric Propulsion Conference*, IEPC-01-57, 2001.

[6] Tamida, T., Osuga, H., Yamamoto, N., Takegahara, H., Aoyagi, J. & Kuriki, K., "Performance Improvement of Hall Thrusters Using a Pulse-Synchronous Driver System," *Journal of Propulsion and Power*, **31**, 956–961, 2015.

[7] Yamamoto, N., Ito, T., Takegahara, H., Watanabe, H., Kuriki, K., Tamida, T. & Osuga, H., "Thrust Performance in Hall Thruster with Pulsating Operation," *34th International Electric Propulsion Conference*, IEPC-2015-213, 2015.

[8] Yamamoto, N., Takegahara, H., Aoyagi, J., Kuriki, K., Tamida, T. & Osuga, H., "Development of a Novel Power Processing Unit for Hall Thrusters," *33rd International Electric Propulsion Conference*, IEPC-2013-248, 2013.